Pergamon

J. Biomechanics, Vol. 28, No. 10, pp. 1167–1177, 1995

0021-9290/95 $9.50 + .00

0021-9290(94)00174-X

FINITE ELEMENT STRESS ANALYSIS OF LEFT VENTRICULAR MECHANICS IN THE BEATING DOG HEART

Julius M. Guccione,* Kevin D. Costa† and Andrew D. McCulloch†

*Department of Mechanical Engineering, Washington University, St Louis, MO 63130-4899; and †Institute for Biomedical Engineering, The University of California, San Diego, La Jolla, CA 92093-0412, U.S.A.

Abstract—A three-dimensional finite element model was used to explore whether or not transmural distributions of end-diastolic and end-systolic fiber stress are uniform from the apex to the base of the canine left ventricular wall. An elastance model for active fiber stress was incorporated in an axisymmetric model that accurately represented the geometry and fiber angle distribution of the anterior free wall. The nonlinear constitutive equation for the resting myocardium was transversely isotropic with respect to the local fiber axis. Transmural distributions of end-diastolic fiber stress became increasingly nonuniform from midventricle toward the apex or the base. At a typical diastolic left ventricular pressure (1 kPa), the differences between largest and smallest fiber stresses were only 0.5 kPa near midventricle, compared with 4.6 kPa at the apex, and 3.3 kPa at the base. Transmural fiber stress differences at end-systole (14 kPa) were relatively small in regions from the base to the midventricle (13–22 kPa), but were larger between midventricle and the apex (30–43 kPa). All six three-dimensional end-diastolic strain components were within or very close to one standard deviation of published measurements through the midanterior left ventricular free wall of the passive canine heart [Omens *et al.*, *Am. J. Physiol.* **261**, H918–H928 (1991)]. End-systolic in-plane normal and shear strains also agreed closely with published experimental measurements in the beating dog heart [Waldman *et al.*, *Circ. Res.* **63**, 550–562 (1988)]. The results indicate that, unlike in the midventricle region that has been studied most fully, there may be significant regional nonhomogeneity of fiber stress in the normal left ventricle associated with regional variations in shape and fiber angle.

Keywords: Myocardium; Systole; Time-varying elastance; Myofiber stress.

INTRODUCTION

Knowledge of the stress distributions in the intact myocardium can provide useful insight into normal ventricular function, since regional coronary blood flow (Jan, 1985), myocardial oxygen consumption (Sarnoff *et al.*, 1958), hypertrophy (Alpert, 1971), and remodeling (Fung, 1990) are all influenced by ventricular wall stress (Yin, 1981). Regional distributions of three-dimensional deformation in the ventricular wall have been measured from the displacements of closely spaced markers that are either implanted in the myocardium (Omens *et al.*, 1991; Waldman *et al.*, 1988) or generated using noninvasive magnetic resonance tagging techniques (McVeigh and Zerhouni, 1991; Young and Axel, 1992). However, the direct measurement of local forces or stresses in the intact heart wall has not been reliable (Huisman *et al.*, 1980). An alternative approach to determine ventricular wall stress is mathematical modeling based on the conservation laws of continuum mechanics (Bergel and Hunter, 1979).

Previously, we and others have used cylindrical, anisotropic, finite elastic models to compute transmural distributions of three-dimensional stresses with respect to the muscle fiber architecture of the intact myocardium at end-diastole (Guccione *et al.*, 1991; Humphrey and Yin, 1989) and at end-ejection (Guccione *et al.*, 1993; Taber, 1991). However, cylindrical models are probably confined at best to describing the mechanics of a narrow equatorial cross-section of the left ventricular wall. Therefore, the purpose of this paper was to extend these models to an axisymmetric geometry that allowed us to compute transmural distributions of end-diastolic and end-systolic fiber stress from the apex to the base of the canine left ventricular wall. We used a three-dimensional finite element model with a longitudinal cross-section based on the free wall anatomy of the canine left ventricle and a realistic muscle fiber distribution.

One assumption of most previous ventricular models has been that the resting material properties of the ventricular wall are homogeneous, apart from the effects of variations in muscle fiber orientation. For many years, transmural variations in material properties have been proposed as a mechanism for permitting uniform wall stress (Janz and Waldron, 1976). However, experimental data on regional variations in

Received in final form 17 *November* 1994.
Address correspondence to: Julius M. Guccione, Ph.D., Washington University, Campus Box 1185, One Brookings Drive, St Louis, MO 63130-4899, U.S.A.

the anisotropic elastic and contractile properties of myocardium are scarce. Recently, Novak *et al.* (1994) reported significant transmural differences in the stored energy of biaxially loaded passive canine left ventricular myocardium. But these differences were modest (only 14% for an equibiaxial stretch of 25%) and the degree of anisotropy was not significantly different between regions. In this paper, we compare finite element model computations of transmural strain distributions with experimental measurements in the resting dog left ventricle (Omens *et al.*, 1991). This allowed us to investigate whether the observed nonhomogeneous distributions of three-dimensional strain were consistent with the assumption of homogeneous material properties when the nonuniform fiber angles and geometry of the left ventricle were included in the analysis.

In the working heart, transmural deformations are also nonhomogeneous and characterized by significant transverse shearing at end-systole (Waldman *et al.*, 1988). Since the cylindrical models could only inflate, stretch and twist, they were not able to produce these transverse shear strains. Therefore, another objective of this paper was to compare the transmural distributions of three-dimensional systolic strain in the intact heart with the results of a model that has nonuniform geometry and muscle fiber angles but no transmural variations in regional systolic elastance (Waldman *et al.*, 1988).

METHODS

Our finite element method was developed specifically for continuum analysis of the heart (Guccione and McCulloch, 1991; Hunter and Smaill, 1988) and includes several features uncommon to conventional methods. The Galerkin finite element equations for three-dimensional finite elasticity (virtual work formulation) were derived in prolate spheroidal coordinates, allowing the ventricular geometry and boundary conditions to be modeled more simply and efficiently. Conforming isoparametric finite elements were used with three-dimensional tensor-product basis functions for each of the prolate spheroidal coordinates. The Galerkin finite element formulation of the virtual work principle is given by equations (18) and (19) of Hunter and Smaill (1988). Our implementation includes some minor modifications to the finite element equations to improve the convergence and accuracy of some solutions. The nonlinear system of global equilibrium equations was solved, subject to pressure and displacement boundary conditions, for the unknown nodal displacement and hydrostatic pressure parameters at each load step using Newton iteration (Gill *et al.*, 1981). The material anisotropy of the ventricular wall was defined by referring the stress tensor components at every point in the element to an orthogonal system of local material coordinates, having one axis aligned with the muscle fiber direction.

The Cartesian coordinates (x, y, z) of a point at (λ, μ, θ) in a prolate spheroidal system with focal length d (Fig. 1A) are given by

$$x = d \cosh \lambda \cos \mu,$$

$$y = d \sinh \lambda \sin \mu \cos \theta,$$

$$z = d \sinh \lambda \sin \mu \sin \theta.$$

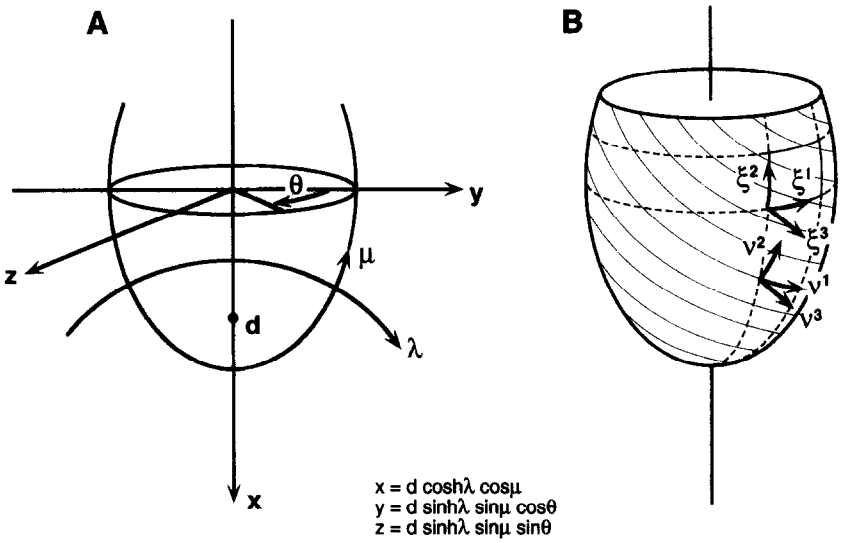

Fig. 1. Cardiac prolate spheroid coordinate system. (A) Prolate spheroid coordinate system (λ, μ, θ) in region to rectangular coordinates (x, y, z); d is focus. (B) Element material coordinates (ξ^1, ξ^2, ξ^3) lie in circumferential, azimuthal, and radial directions, respectively, whereas (v^1, v^2, v^3) lie in fiber, cross-fiber, and radial directions, respectively.

Some previous ventricular mechanics models have used spherical (Abe and Nakamura, 1982) or cylindrical coordinates which have focal lengths of zero and infinity, respectively. Surfaces of constant λ form ellipsoids of revolution about the x-axis. Figure 1B shows the local finite element material coordinates (ξ^1, ξ^2, ξ^3) which each range from 0 to 1, in every element. To model the muscle fiber orientations, we assume that the fibers lie in the (ξ^1, ξ^2)-coordinate plane. The fiber coordinates (v^1, v^2, v^3) also shown in Fig. 1B are orthogonal in the undeformed state, with v^1 aligned with the local fiber direction and v^2 perpendicular to it in the (ξ^1, ξ^2) plane, parallel to the wall. The fiber and finite element coordinates are both convecting.

The axisymmetric geometry of the left ventricular model was obtained from the three-dimensional anatomical measurements of the unloaded canine heart made by Nielsen *et al.* (1991), who used least squares to fit a prolate spheroidal finite element mesh with 24 higher-order elements and 41 nodes to within 2.1 mm of 576 epicardial and 360 endocardial left ventricular measurements. Figure 2 shows a longitudinal cross-section of a 14-element trilinear axisymmetric model

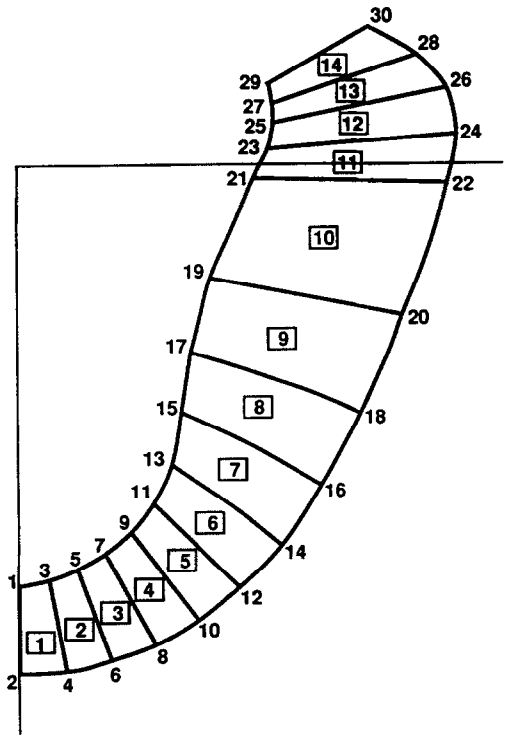

Fig. 2. Unloaded reference state of 14-element axisymmetric model fitted by least squares to extensive anatomical measurements (Nielsen *et al.*, 1991) from a cross-section of the anterior free wall in the canine left ventricle fixed at zero transmural pressure. Ventricular cavity volume 37 ml; wall volume 125 ml. Prolate spheroidal nodal coordinates and fiber angle values are listed in Table 1.

derived from the prolate spheroidal coordinates of the Nielsen *et al.* three-dimensional model at a lateral section of the left ventricular free wall. Trilinear finite element interpolation of the prolate spheroidal coordinates [equation (1) of Nielsen *et al.*, 1991] with nine Gaussian quadrature points (Zienkiewicz and Morgan, 1982) was sufficient to integrate the element volumes exactly. Spatial refinement was sufficient to guaranteee convergence of the strain energy to within 10% as we have demonstrated in detail previously (see Guccione and McCulloch, 1991). Nielsen *et al.* (1991) also fitted the distributions of ventricular muscle fiber orientations to 8690 measurements throughout the ventricular walls with a root mean squared error less than 17°. This fiber orientation field was described in the model by assuming that fibers lie in element (ξ^1, ξ^2)-coordinate planes which form the endocardial and epicardial surfaces. The orientation of fibers with respect to the circumferential direction in these planes was described by a bilinear interpolation of nodal parameters, and the transmural variation of fiber angle had a linear Lagrange basis. The nodal parameters of this mesh are listed in Table 1, where a fiber angle (η) of zero corresponds to the circumferential direction and a positive angle is rotated counterclockwise. The focal length in the model was 2.91 cm.

To define the passive material properties of the ventricular wall, we used a strain energy potential W that was an exponential function of strain components $E_{\alpha\beta}$ referred to fiber v^α-coordinates:

$$W = \frac{C}{2}(e^Q - 1) \quad \text{and} \quad E_{\alpha\beta} = \frac{1}{2}\left(\frac{\partial x^k}{\partial v^\alpha}\frac{\partial x^k}{\partial v^\beta} - \delta_{\alpha\beta}\right), \quad (1)$$

where

$$Q = b_f E_{11}^2 + b_t(E_{22}^2 + E_{33}^2 + E_{23}^2 + E_{32}^2) + b_{fs}(E_{12}^2 + E_{21}^2 + E_{13}^2 + E_{31}^2),$$

x^k are deformed rectangular Cartesian coordinates and $\delta_{\alpha\beta}$ is the Kronecker delta. E_{11} is fiber strain, E_{22} is cross-fiber in-plane strain, E_{33} is radial strain, E_{23} is shear in the transverse plane, and E_{12} and E_{13} are shear strain in fiber–cross fiber and fiber–radial coordinate planes, respectively. Since the fiber coordinates are locally orthonormal, these covariant strain components are also physical components. The form of Q describes a material that is transversely isotropic with respect to the muscle fiber axis (Guccione *et al.*, 1991). Previously, we found that the material constants $C = 0.876$ kPa, $b_f = 18.48$, $b_t = 3.58$, $b_{fs} = 1.627$ allowed a cylindrical model of the left ventricle to match epicardial strains measured in an intact canine heart preparation (McCulloch *et al.*, 1989) during passive left ventricular filling. That analysis and biaxial testing of thin sheets from the left ventricular free wall (Novak *et al.*, 1994) both indicate

Table 1. Nodal parameters for a 14-element axisymmetric model

Node	λ	μ (deg)	n (deg)
1	0.699	0.0	96.8
2	0.982	0.0	− 52.9
3	0.689	6.7	95.9
4	0.984	6.7	− 51.5
5	0.685	13.5	95.0
6	0.986	13.5	− 50.1
7	0.682	20.2	94.1
8	0.989	20.2	− 48.5
9	0.676	27.0	93.3
10	0.991	27.0	− 46.9
11	0.664	34.0	92.4
12	0.992	34.0	− 45.1
13	0.635	42.0	91.3
14	0.992	42.0	− 43.0
15	0.589	51.0	89.9
16	0.989	51.0	− 43.2
17	0.559	61.0	88.5
18	0.995	61.0	− 44.8
19	0.565	73.0	87.3
20	1.017	73.0	− 46.8
21	0.655	88.0	86.2
22	1.072	88.0	− 49.2
23	0.693	92.1	85.6
24	1.092	93.0	− 48.7
25	0.710	95.6	84.6
26	1.081	98.0	− 46.8
27	0.712	98.4	98.4
28	1.035	102.0	− 44.9
29	0.707	101.1	82.3
30	0.949	106.0	− 42.5

that the normal passive tissue is several times stiffer in the fiber direction than in the transverse plane.

Systolic contraction was modeled by defining the second Piola–Kirchhoff stress tensor referred to fiber v^α-coordinates in the undeformed body as the sum of the passive three-dimensional stress derived from the strain energy function and an active fiber-directed component T_0, which was a function of time t, peak intracellular calcium concentration Ca_0, and sarcomere length l (Guccione *et al.*, 1993):

$$t^{\alpha\beta} = \frac{1}{2}\left(\frac{\partial W}{\partial E_{\alpha\beta}} + \frac{\partial W}{\partial E_{\beta\alpha}}\right) - pg^{\alpha\beta} + T_0(t, Ca_0, l)\delta_1^\alpha \delta_1^\beta, \tag{2}$$

where the contravariant metric tensor referred to fiber coordinates $g^{\alpha\beta} = (\partial v^\alpha/\partial x^k)(\partial x^\beta/\partial x^k)$. We introduced the hydrostatic pressure p as the Lagrange multiplier needed to enforce the kinematic constraint that the third principal strain invariant (I_3) equals one. The relations between T_0, t, Ca_0, and l are given by equations (8)–(12) of Guccione *et al.* (1993). Sarcomere length is related to fiber strain by the following relation:

$$l = l_R\sqrt{2E_{11} + 1}, \tag{3}$$

where l_R is the sarcomere length in the unloaded reference configuration. The Cauchy stress tensor referred to new locally orthonormal fiber $\hat{v}^i$-coordinates in the deformed body and the second Piola–Kirchhoff stress tensor are related by the transformation

$$T^{ij} = \frac{\partial x^k}{\partial v^\alpha}\frac{\partial x^l}{\partial v^\beta}\frac{\partial \hat{v}^i}{\partial x^k}\frac{\partial \hat{v}^j}{\partial \partial x^l}t^{\alpha\beta}\frac{1}{\sqrt{I_3}}. \tag{4}$$

Although the fiber coordinates are curvilinear in general, orthonormal scaling of the base vectors means that T^{ij} represent physical components of stress. Figure 3 shows predicted passive and end-systolic fiber stresses (T^{11}) plotted as a function of sarcomere length for the case of uniform extension in the fiber direction.

The parameters of the active contraction model were based on experimental measurements of sarcomere length and tension in isolated rat trabeculae (see Guccione *et al.*, 1993). They are listed in Table 1 of Guccione *et al.* (1993). A more complete model should include the deactivating effects of shortening velocity and history dependence in cardiac muscle (Guccione and McCulloch, 1993), but it has been shown that a 'time-varying elastance model' such as the present one is suitable for modeling the mechanics of ventricular contracton at end-systole (Guccione *et al.*, 1993). This observation is consistent with the well-known observation that the pressure developed by the ventricles at end-systole is largely independent of the ejection history or rate; it depends only on the end-systolic volume (Sagawa *et al.*, 1988).

To simulate a beating left ventricle, the model was loaded passively by an end-diastolic pressure of 0.63 kPa and contracted actively against an end-systolic pressure of 14 kPa (experimental means from Waldman *et al.*, 1988). End-systole occurred 350 ms after the end of diastole (see Guccione *et al.*, 1993).

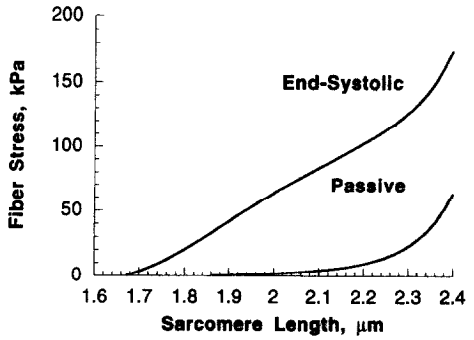

Fig. 3. Computed passive and end-systolic fiber stresses plotted as a function of sarcomere length for the case of uniform extension in the fiber direction when $l_R = 1.85$ μm. In the unloaded reference model configuration, l_R varies linearly from 1.78 μm (endocardium) to 1.91 μm (epicardium).

The effects of residual stress on sarcomere length and hence systolic ventricular mechanics were included in the model by assuming a linear transmural variation in sarcomere length from 1.78 μm (endocardium) to 1.91 μm (epicardium) in the unloaded state, in accordance with recent experimental observations (Rodriguez *et al.*, 1993). All three deformed prolate spheroidal nodal coordinates were interpolated using trilinear basis functions and, hence, the hydrostatic pressure variable was constant in each element to satisfy the compatibility condition of this mixed formulation. Circumferential and azimuthal displacements were constrained at all nodes at the base during both filling and ejection. Radial displacement of the basal epicardial nodes was constrained during filling to simulate the restricted dilation of the valve annuli imposed by the stiff collagenous valve rings. During ejection, however, radial contraction was not prevented at the base because enforcing the constraint led to large stress concentrations.

For adequate convergence of solutions for the steep transmural variations in deformation occurring within the contracting model, the original 14-element mesh in Fig. 2 was subdivided into four elements transmurally. In addition, the four most apical elements (element 1 in the original mesh) were adjusted (constrained at $\mu = 3°$) to avoid numerical ill-conditioning due to the singularity at the apex. In other words, there was a small hole in the apex between $\mu = 0°$ and $\mu = 3°$. Model simulations of passive left ventricular filling required 5 min on a Silicon Graphics Indigo^2 Extreme Graphics workstation with 32 MB of RAM, whereas simulations of end-systolic ventricular mechanics required 20 min. The stress and strain solutions from a more refined mesh with eight elements transmurally and 28 elements longitudinally were not significantly different.

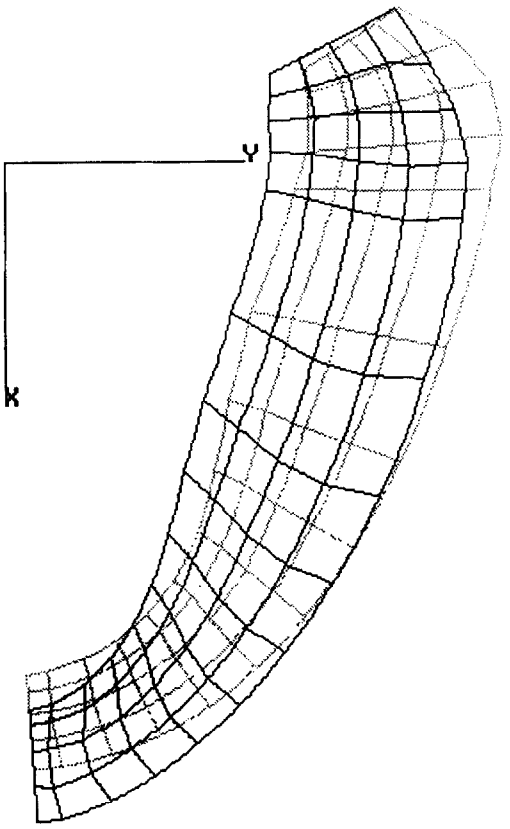

Fig. 4. End-diastolic (dotted lines) and end-systolic (solid lines) configurations of a 56-element axisymmetric model obtained by twice subdividing the 14-element mesh transmurally after adjusting the apical element (see text). Comparison shows substantial wall thickening throughout longitude and significant longitudinal–radial shearing in apical subendocardial region during systole. End-diastolic cavity volume 40 ml; end-systolic cavity volume 39 ml.

RESULTS

The cavity volumes of the finite element mesh in the filling and ejecting states (Fig. 4) were 49 and 39 ml, respectively, yielding an ejection fraction of 20%. This is consistent with the depressed cardiac function typical of the open-chest pentabarbitol-anesthetized animal. Comparing the end-diastolic and end-systolic model configurations shows that there was substantial wall thickening throughout the longitude as well as significant longitudinal–radial shearing in the apical subendocardial region during systole. Also, the model twisted during ejection in the opposite sense to that seen in filling (not shown).

During passive inflation, transmural distributions of fiber stress became increasingly nonuniform from midventricle toward the apex and the base (Fig. 5). At a left ventricular pressure of 1 kPa, the difference between the largest and smallest fiber stresses was a maximum of 4.6 kPa at the apex (ignoring the most apical row of elements which showed transmural oscillations due to incomplete convergence), a minimum of 0.5 kPa a near midventricle (elements 8 and 9 of the original mesh), and 3.3 kPa at the base. Throughout the longitude, fiber stress was greatest at the subendocardium and smallest in the midwall, with the exception of the most apical region (original elements 2–4) where it was smallest in the subepicardium.

All six three-dimensional passive strain components were within or very close to one standard deviation of the measurements by Omens *et al.* (1991) through the midanterior left ventricular free wall of the isolated, potassium-arrested dog heart (Fig. 6). Circumferential strain (A) and transmural wall thinning (C) both decreased from subendocardium to epicardium, consistent with experiment. Longitudinal strain (B) was similar to experiment at the midwall, but was smaller at the subendocardium and larger at the subepicardium. The model matched the small negative in-plane shear strains (D), which are consistent with a left-handed torsion of the left ventricular wall during passive filling, and the small transverse shear in the longitudinal–radial plane (F). However,

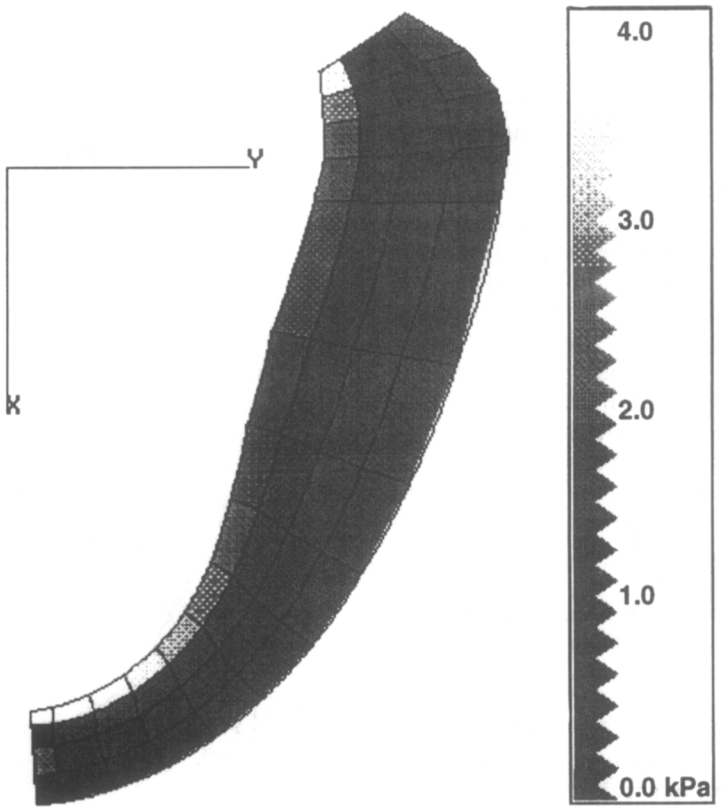

Fig. 5. Gray-scale map of fiber stress at end-diastole obtained from the center of each element in the model. Transmural distributions of fiber stress became increasingly nonuniform from midventricle toward the apex and the base. Left ventricular pressure 1 kPa.

the model predicted negative circumferential–radial transverse shears (E) at the midwall which were not observed experimentally. When the strains were referred to local fiber coordinates, all three normal strain components were found to agree well with the measurements, and the only major discrepancy occurred in the subendocardial prediction of fiber–cross-fiber shear strain.

Transmural distributions of end-systolic fiber stress were relatively uniform between the base and midventricle, but not between midventricle and the apex (Fig. 7). At a left ventricular pressure of 14 kPa, the differences between largest and smallest fiber stresses were 30–43 kPa between the apex and midventricle (element 2–7 of the original mesh) and 13–22 kPa between midventricle and the base (original elements 8–13). The epicardial stress concentration at the base (original element 14) is probably artifactual. Throughout the longitude, fiber stress was smallest in the midwall and greatest in the subendocardium, with the exception of the most basal region (original elements 12–14) where it was greatest in the subepicardium.

Only the end-systolic strain components in the plane of the wall agreed with experimental measurements by Waldman *et al.* (1988) through the midanterior left ventricular free wall of the open-chest anethetized dog (Fig. 8). Transmural distributions of circumferential (A) and longitudinal (B) end-systolic strains agreed very well with the experimental data, whereas the radial strain component obtained by the model uniformly overestimated the data (C). The in-plane shear strain distribution was also quite reasonable (D), but the circumferential–radial (E) and longitudinal–radial (F) transverse shear strains were fundamentally different from experimental values.

DISCUSSION

We used a three-dimensional finite element model of the canine left ventricle with a long-axis geometry and muscle fiber distribution based on published measurements for the anterior free wall to compute regional distributions of muscle fiber stress at end-diastole and end-systole. Although the hypothesis of a uniform fiber stress distribution is an attractive theory of optimal myocardial function (Arts *et al.*, 1982; Fung, 1984; Guccione *et al.*, 1991), our results suggest that transmural fiber stress distributions may vary significantly along the longitude of the ventricular wall, especially between midventricle and the apex.

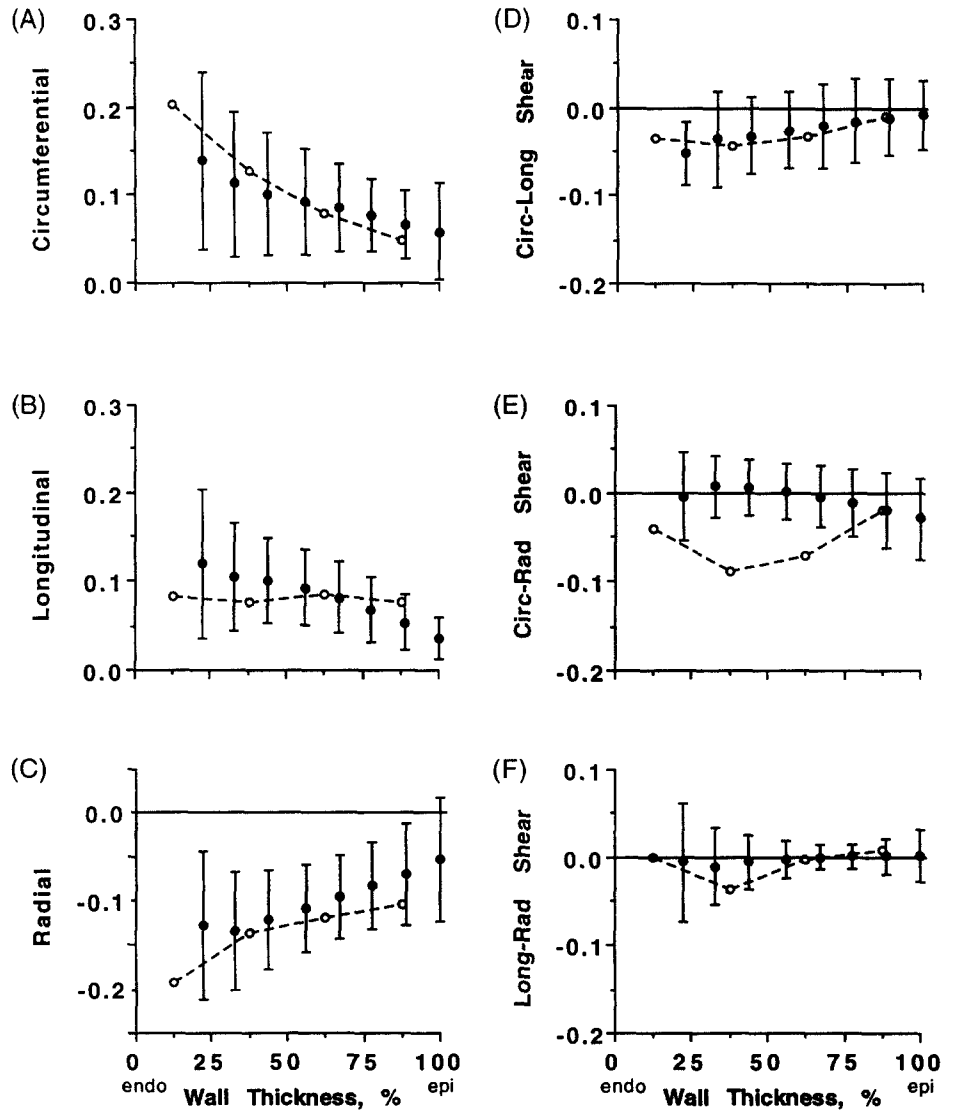

Fig. 6. End-diastolic finite strain distributions from the midventricular region of the finite element model (open symbols) are consistent with three-dimensional strain measurements for passive inflation (Omens *et al.*, 1991). Except for the circumferential–radial shear strain (panel E), all model predictions are within 1 S.D. (error bars) of the experimental means (filled symbols). Strains are referred to the unloaded configuration. Note that lines connecting the open symbols are not model predictions. Left ventricular pressure 1 kPa.

The distributions of fiber stress are consistent with the regional geometry and fiber angles in our model. When the thick-walled left ventricle is inflated passively, the greatest deformations occur at the endocardium where the pressure load is applied. Near the midventricle, where longitudinal curvature is low, circumferential strain exceeds longitudinal strain. In the more spherical apical and basal regions, however, the two components are more similar. At the midventricle, this dominance of circumferential and endocardial strains during filling combines to result in a relatively uniform distribution of fiber stress and strain because the fiber orientation changes from near longitudinal at the endocardium to circumferential near the midwall (Guccione *et al.*, 1991). Since this same general distribution of fiber angles occurs throughout the long axis of the ventricle, the tendency for the in-plane strains to become more biaxial as circumferential and longitudinal curvatures become more equal away from the midventricle also gives rise to less uniform fiber stress and strain across the wall. End-systolic fiber stress distributions are more difficult to interpret because of the additional active contractile component. Our model suggests that active contraction tends to make these distributions more uniform in the basal region and much less so between midventricle and the apex.

The generally good agreement between model results of transmural three-dimensional strain distributions and experimental measurements from the left

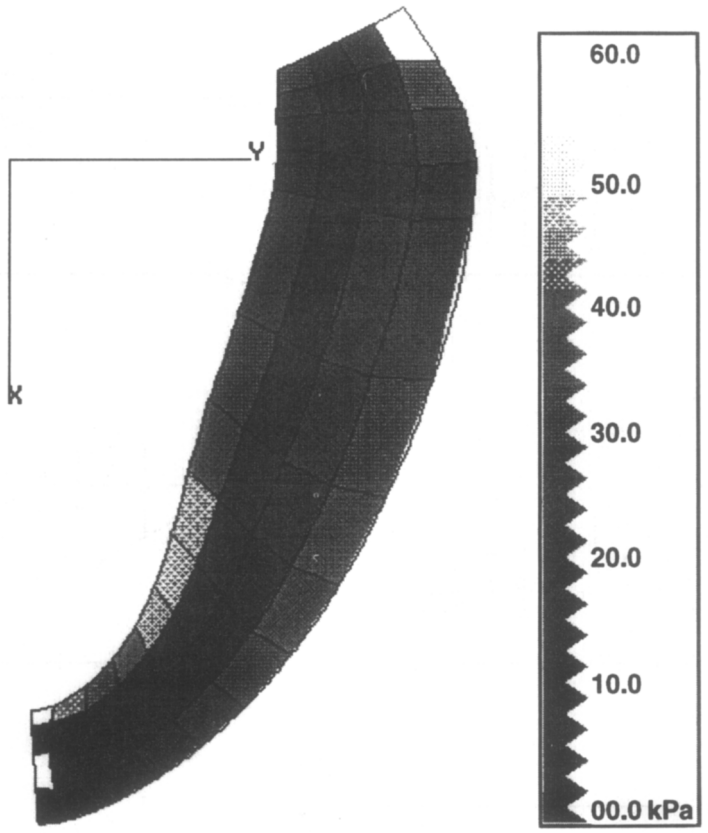

Fig. 7. Gray-scale map of fiber stress at end-systole obtained from the center of each element in the model. Transmural distributions of fiber stress are relatively uniform between the base and midventricle, but not between midventricle and the apex. Left ventricular pressure 14 kPa.

ventricular free wall of the passive dog heart (Omens *et al.*, 1991) helps to confirm the validity of the end-diastolic fiber stresses in the model. Because the agreement between computed and measured circumferential–radial shear strain is significantly better in the subendocardium and subepicardium than at midwall, and the computed longitudinal strain does not exhibit the observed transmural variation, model findings may be improved by allowing the material constants C, b_f, b_t, b_{fs} in equation (1) to vary transmurally. In a detailed study on the regional multiaxial stress–strain behavior of passive myocardium, Novak *et al.* (1994) found that biaxial specimens from the inner and outer portions of the left ventricular free wall tended to be slightly stiffer than those from the middle of the septum and free wall. However, it is difficult to obtain more than two viable specimens from the same heart, and the extent to which these results reflect the material properties of *intact* myocardium remains uncertain. Moreover, measurements of passive myocardial strain from apex to base are needed to determine whether these material constants may also vary longitudinally. Recent observations of variations in connective tissue organization from apex to base as well as around the circumference of the ventricular walls (Hunter *et al.*, 1993) suggest that passive myocardial material properties vary significantly in three dimensions. Since it would be extremely difficult to estimate material parameters from regional strain measurements while allowing the parameters to vary in three dimensions, a new approach to mechanical testing of intact myocardium that allows for regional determination of transmural variations in material properties (currently being undertaken in our laboratory) would be worthwhile.

In contrast, the inability of the model to accurately reproduce all of the three-dimensional strain components observed at end-systole suggests that at least some of the three-dimensional stress solutions are also not accurate, and there is no guarantee that any of them are correct because in general all the strain components contribute to every stress component. Nevertheless, the generally good agreement between transmural distributions of three-dimensional *in-plane* strains in the model and experimental measurements in the beating dog heart (Waldman *et al.*, 1988) adds support to the systolic fiber stress distributions. Fiber stress dominated all other stress components throughout the model. The compressive cross-fiber stress never exceeded 15 kPa in magnitude, and the radial stress was governed by the applied pressure loads. Shear stress components were small and, except

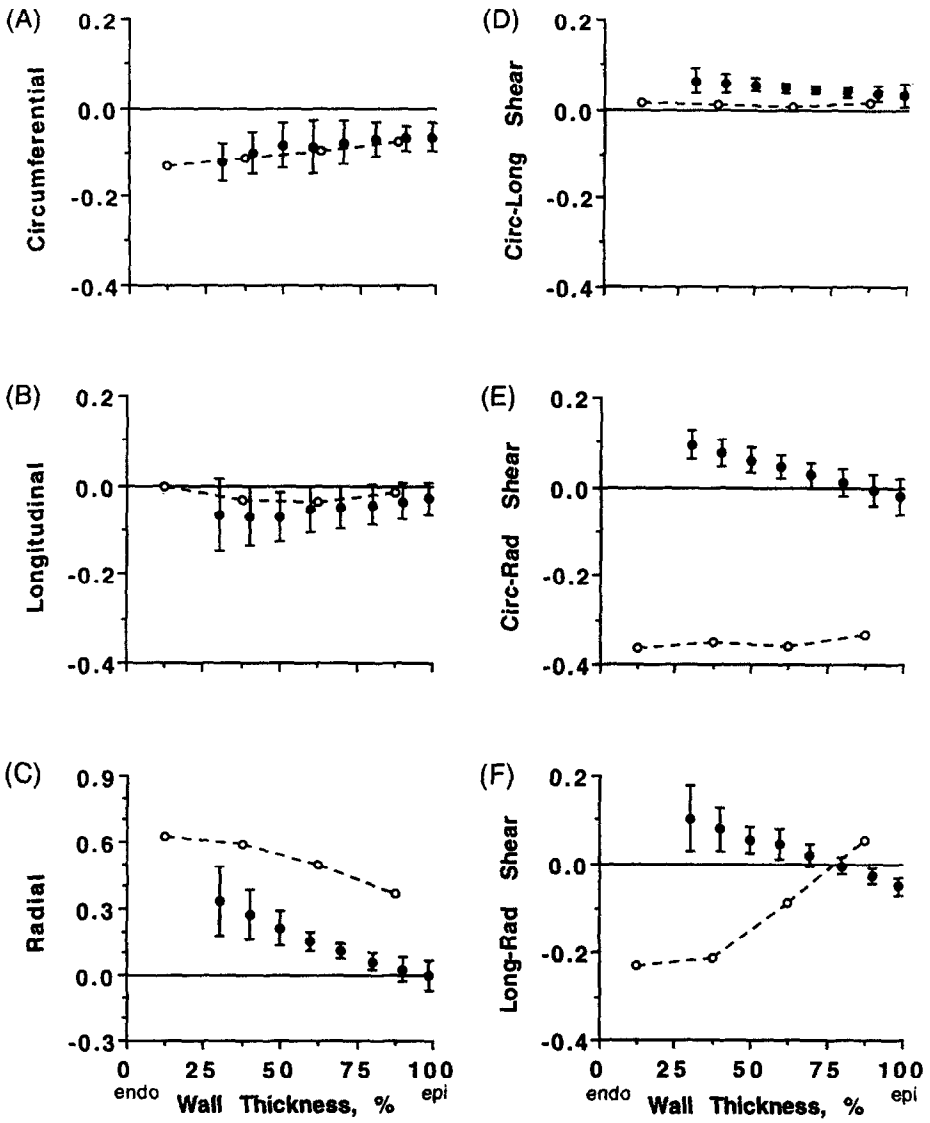

Fig. 8. Comparison of experimental end-systolic strains with those predicted by the model (open symbols). Only the in-plane components agree with experimental data (filled symbols) of Waldman *et al.* (1988). Strains are referred to end-diastole. Left ventricular pressure 14 kPa.

for the fiber–radial component near the apex, none exceeded 5 kPa in magnitude. The active fiber stress was responsible for 75–90% of the fiber stress at end-systole in the same region where the measured transverse shear strains disagreed with the model results. Moreover, fiber strain dominated the passive stress so the net contribution of other strain components must be quite minor. In our elastance model for active fiber stress, tension development at end-systole depends entirely on local sarcomere length. The model computations of end-systolic sarcomere length depend on the unloaded length and the deformation in the epicardial tangent plane from end-diastole to the end of ejection, which agreed with the experimental measurements of Waldman *et al.* (1988). In order to account for the effects of residual stress on systolic ventricular mechanics, the sarcomere length distribution in the unloaded model was assumed to vary linearly between 1.78 μm (endocardium) and 1.91 (epicardium) in accordance with experimental data from the potassium-arrested rat heart (Rodriguez *et al.*, 1993). It is uncertain whether this transmural distribution holds from apex to base. Even when the unloaded sarcomere length distribution was assumed to be uniform, however, the differences in model computations of fiber stress were negligible.

Part of the discrepancy in predicted and measured radial strains may reflect the effect of altered coronary blood volume during the cardiac cycle due to the phase difference between coronary artery and venous flow (Canty Jr and Brooks, 1990). Whereas the model deformations were constrained to be strictly isochoric, the experimental measurements suggest a loss of wall volume during systole. One explanation for the signi-

ficant discrepancy in computed and measured transverse shear strains may be that contraction of the papillary muscles was not included in the model. A recent preliminary study on two open-chest anesthetized dogs (Takayama *et al.*, 1994) suggests that at end-systole, chordal transection increases longitudinal–radial shear in the anterior papillary muscle and inner wall. However, coronary blood volume is only a small percentage of the total wall volume, and the effects of papillary muscle contraction should be confined to a small region surrounding their insertion into the ventricular wall. On the other hand, the transverse laminar structures described by Smaill and Hunter (Hunter *et al.*, 1993; Smaill and Hunter, 1991) and referred to as cleavage planes by Spotnitz *et al.* (1974) are most likely related directly to transverse shearing and radial deformations throughout the ventricular wall (LeGrice *et al.*, 1994). Hence, our model results suggest that material orthotropy with respect to these transverse laminae may be an important determinant of the transverse shears and radial strains observed in the intact myocardium during systole. To elucidate this relationship new experimental data on the multiaxial orthotropic material properties of myocardium and their relationship to the fiber and laminar organization of the tissue are needed.

Bovendeerd *et al.* (1992) recently proposed a finite element model of the beating left ventricle to investigate the dependence of local mechanics on myocardial muscle fiber orientations. Similar to our approach, they used a three-dimensional finite element method to analyze a model with axisymmetric geometry, boundary conditions and material properties. This three-dimensional description allowed us to study deformations not permitted by strictly axisymmetric models, for example, torsion and circumferential–radial shear. Bovendeerd's axisymmetric analysis of the entire cardiac cycle serves as an important contribution to cardiac mechanics because it accounted for the dependence of active stress on time, strain and strain rate, activation sequence of the left ventricular wall and aortic afterload. The authors did not include their comparisons of modeled myocardial deformations with experimental data in Bovendeerd *et al.* (1992), but they are shown in Fig. 5.2 of Bovendeerd (1990). It is interesting, although not surprising, that Bovendeerd's model also had difficulty predicting the radial and transverse shear strains measured by Waldman *et al.* (1988).

Bovendeerd and co-workers modeled the unloaded left ventricular geometry by a truncated confocal ellipsoid. They concluded that the distributions of active muscle fiber stress and muscle fiber strain across the left ventricular wall are very sensitive to the transmural variation in muscle fiber orientation, but a physiological transmural fiber angle distribution can be found that gives rise to approximately homogeneous distributions of these stress and strain components. Our model incorporated a wall geometry and fibrous architecture fitted to extensive measurements from the left ventricle, and yielded less uniform distributions of end-systolic sarcomere length and fiber stress at end-systole.

Unlike in the midventricle region that has been studied most fully, there may be significant regional heterogeneity of fiber stress and strain in the normal left ventricle associated with regional variations in shape and fiber angle. Hence, the hypothesis of uniform fiber stress and strain may need to be modified or other mechanisms not included in the model such as regional variations in residual stress or material properties may be physiologically important. Alternatively, this heterogeneity may confer some functional advantage on myocardial performance.

Acknowledgements—We are grateful to Professor Peter J. Hunter, who initiated the development of our finite element models of the heart and has continued to extend the scope of the methods over the past 10 years. We would also like to thank Professors Y.-C. Fung, Poul M. F. Nielsen, and Lewis K. Waldman for their valuable advice and contributions to this work. This research was supported by NIH Grants HL41603 (A. D. McCulloch) and HL43026 (S. Chien), NSF Grant BCS-9157961 (A. D. McCulloch) and grants from the Whitaker Foundation (J. M. Guccione, A. D. McCulloch). This support is gratefully acknowledged.

REFERENCES

Abe, H. and Nakamura, T. (1982) Finite deformation model for the mechanical behavior of left ventricular wall muscles. *Math. Modeling* **3**, 143–152.

Alpert, N. R. (1971) *Cardiac Hypertrophy*. Academic Press, New York.

Arts, T., Veenstra, P. C. and Reneman, R. S. (1982) Epicardial deformation and left ventricular wall mechanics during ejection in the dog. *Am. J. Physiol.* **243**, H379–H390.

Bergel, D. A. and Hunter, P. J. (1979) The mechanics of the heart In *Quantitative Cardiovascular Studies* (Edited by Hwang, N. H. C., Gross, D. R. and Patel, D. J.), pp. 151–213. University Park Press, Baltimore.

Bovendeerd, P. H. M. (1990) The mechanics of the normal and ischemic left ventricle during the cardiac cycle: a numerical and experimental analysis. Ph.D. thesis, University of Limburg, Maastricht, The Netherlands.

Bovendeerd, P. H. M., Arts, T., Huyghe, J. M., van Campen, D. H. and Reneman, R. S. (1992) Dependence of local left ventricular wall mechanics on myocardial fiber orientation: a model study. *J. Biomechanics* **25**, 1129–1140.

Canty, J. M. Jr and Brooks, A. (1990) Phasic volumetric coronary venous outflow patterns in conscious dogs. *Am. J. Physiol.* **258**, H1457–1463.

Fung, Y. C. (1984) *Biodynamics: Circulation*. Springer, New York.

Fung, Y. C. (1990) *Biomechanics: Motion, Flow, Stress and Growth*. Springer, New York.

Gill, P. E., Murray, W. and Wright, M. H. (1981) *Practical Optimization*. Academic Press, London.

Guccione, J. M. and McCulloch, A. D. (1991) Finite element modeling of ventricular mechanics. In *Theory of Heart: Biomechanics, Biophysics, and Nonlinear Dynamics of Cardiac Function* (Edited by Glass, L., Hunter, P. J. and McCulloch, A. D.), pp. 121–144, Springer, New York.

Guccione, J. M. and McCulloch, A. D. (1993) Mechanics of active contraction in cardiac muscle: Part I—constitutive relations for active fiber stress that describe deactivation. *ASME J.biomech. Engng* **115**, 72–81.

Guccione, J. M., McCulloch, A. D. and Waldman, L. K. (1991) Passive material properties of intact ventricular myocardium determined from a cylindrical model. *ASME J. biomech. Engng* **113,** 42–55.

Guccione, J. M., Waldman, L. K. and McCulloch, A. D. (1993) Mechanics of active contraction in cardiac muscle: Part II—cylindrical models of the systolic left ventricle. *ASME J. biomech. Engng* **115,** 82–90.

Huisman, R. M., Elzinga, G., Westerhof, N. and Sipkema, P. (1980) Measurement of left ventricular wall stress. *Cardiovasc. Res.* **14,** 142–153.

Humphrey, J. D. and Yin, F. C. P. (1989) On constitutive relations and finite deformatioins of passive cardiac tissue: II. Stress analsyis in the left ventricle. *Circ. Res.* **65,** 805–817.

Hunter, P. J., Nielsen, P. M. F., Smaill, B. H., LeGrice, I. J. and Hunter, I. W. (1993) An anatomical heart model with applications to myocardial activation and ventricular mechanics. In *High-Performance Computing in Biomedical Research* (Edited by Pilkington, T. C., Loftis, B., Thompson, J. F., Woo, S. L.-Y., Palmer, T. C. and Budinger, T. F.), pp. 3–26. CRC Press, Boca Raton.

Hunter, P. J. and Smaill, B. H. (1988) The analysis of cardiac function: a continuum appraoch. *Prog. Biophys. Molec. Biol.* **52,** 101–164.

Jan, K.-M. (1985) Distribution of myocardial stress and its influence on coronary blood flow. *J. Biomechanics* **18,** 815–820.

Janz, R. F. and Waldron, R. J. (1976) Some implications of a constant fiber stress hypothesis in the diastolic left ventricle. *Bull. Math. Biol.* **38,** 401–413.

LeGrice, I. J., Takayama, Y. and Covell, J. (1994) Transverse shear along myocardial cleavage planes provides a mechanism for normal systolic wall thickening. *Circulation* **88** (Suppl.), I-630.

McCulloch, A. D., Smaill, B. H. and Hunter, P. J. (1989) Regional left ventricular epicardial deformation in the passive dog heart. *Circ. Res.* **64,** 721–733.

McVeigh, E. R. and Zerhouni, E. A. (1991) Noninvasive measurement of transmural gradients in myocardial strain with magnetic resonance imaging. *Radiology* **180,** 677–683.

Nielsen, P. M. F., LeGrice, I. J., Smaill, B. H. and Hunter, P. J. (1991) Mathematical model geometry and fibrous structure of the heart. *Am. J. Physiol.* **260,** H1365–H1378.

Novak, V. P., Yin, F. C. P. and Humphrey, J. D. (1994) Regional mechanical properties of passive myocardium. *J. Biomechanics* **27,** 403–412.

Omens, J. H., May, K. D. and McCulloch, A. D. (1991) Transmural distribution of three-dimensional strain in the isolated arrested canine left ventricle. *Am. J. Physiol.* **261,** H918–H928.

Rodriguez, E. K., Omens, J. H., Waldman, L. K. and McCulloch, A. D. (1993) Effect of residual stress on transmural sarcomere length distributions in rat left ventricle. *Am. J. Physiol.* **264,** H1048–H1056.

Sagawa, K., Maughan, L., Suga, H. and Sunagawa, K. (1988) *Cardiac Contraction and the Pressure–Volume Relationship.* Oxford University Press, New York.

Sarnoff, S. J., Braunwald, E., Welch, G. H. Jr, Case, R. B., Stainsby, W. N. and Macruz, R. (1958) Hemodynamic determinants of oxygen comsumption of the heart with special reference to the tension-time index. *Am. J. Physiol.* **192,** 148–156.

Smaill, B. H. and Hunter, P. J. (1991) Structure and function of the diastolic heart: material properties of passive myocardium. In *Theory of Heart: Biomechanics, Biophysics, and Nonlinear Dynamics of Cardiac Function* (Edited by Glass, L., Hunter, P. J. and McCulloch, A. D.), pp. 1–29. Springer, New York.

Spotnitz, H. M., Spotnitz, W. D., Cottrell, T. S., Spiro, D. and Sonnenblick, E. H. (1974) Cellular basis for volume related wall thickness changes in the rat left ventricle. *J. Mol. Cell. Cardiol.* **6,** 317–331.

Taber, L. A. (1991) On a nonlinear theory for muscle shells: Part II—application to the beating left ventricle. *ASME J. biomech. Engng* **113,** 63–71.

Takayama, Y., LeGrice, I. J., Holmes, J. W. and Covell, J. W. (1994) Effects of chordal uncoupling on deformation in the papillary muscle. *FASEB J.* **8,** A591.

Waldman, L. K., Nosan, D., Villarreal, F. J. and Covell, J. W. (1988) Relation between transmural deformation and local myofiber direction in canine left ventricle. *Circ. Res.* **63,** 550–562.

Yin, F. C. P. (1981) Ventricular wall stress. *Circ. Res.* **49,** 829–842.

Young, A. A. and Axel, L. (1992) Three-dimensional motion and deformation of the heart wall: estimation with spatial modulation of magnetization—a model-based approach. *Radiology* **185,** 241–247.

Zienkiewicz, O. C. and Morgan, K. (1982) *Finite Elements and Approximation.* Wiley, New York.